Colloquium: Quantum networks with trapped ions

L.-M. Duan

Department of Physics, University of Michigan, Ann Arbor, Michigan 48109, USA

C. Monroe

Joint Quantum Institute, University of Maryland Department of Physics and National Institute of Standards and Technology, College Park, Maryland 20742, USA

(Published 28 April 2010)

Quantum computation and communication exploit the quantum properties of superposition and entanglement in order to perform tasks that may be impossible using classical means. In this Colloquium recent experimental and theoretical progress in the generation of entangled quantum networks based on the use of optical photons as carriers of information between fixed trapped atomic ion quantum memories are reviewed. Taken together, these quantum platforms offer a promising vision for the realization of a large-scale quantum network that could impact the future of communication and computation.

DOI: 10.1103/RevModPhys.82.1209 PACS number(s): 03.67.Bg, 03.67.Hk, 42.50.Ex

CONTENTS

I. INTRODUCTION TO QUANTUM NETWORKS

A. The dream of a quantum internet

The world wide web is an indispensable resource for modern society. The information transmitted through the internet is classical in the sense that the information is encoded by a string of bits, each of which is in one of the two definite states, either 0 or 1. In contrast, quantum information can be represented by quantum superposition states, such as $\alpha|0\rangle+\beta|1\rangle$, with arbitrary normalized superposition coefficients α and β. When more than one such quantum bit (qubit) is considered, entangled superposition states such as $\alpha|0\rangle|0\rangle+\beta|1\rangle|1\rangle$ can also be created. Measurements of the entangled qubits result in strong correlations even though the individual qubits are not well defined and may not even have a direct link at the time of measurement. Entangled qubits thus possess an extra connection between memory elements that is absent with classical bits. With clever use of such entangled qubits, superfast computation and secure communication can be achieved within the new discipline of quantum information processing (Nielsen and Chuang, 2000). Given such promising applications, it is natural to consider a quantum internet (Kimble, 2008), whereby entangled quantum states are shared among many nodes, and appropriate measurements may provide new opportunities in communication and computation.

Similar to classical networks, quantum networks consist of distributed processors that are connected through communication channels. Local quantum processors used to store and/or process quantum information are hereby referred to as quantum nodes. Quantum communication channels transfer quantum information between quantum nodes, which may be at distant locations. In practice, quantum communication channels are usually represented by optical photons, as this system can carry quantum information to distant locations at high speed, and optical fibers provide a practical way to guide photon pulses with little disturbance. However, even with the best fibers photon pulses still decay exponentially over distance due to light absorption and scattering, leading to the degradation of the signal. Classically, this is mitigated through the use of repeater circuits, which periodically amplify the signal before any significant degradation. Quantum mechanically, a simple extension of this idea does not work because unknown quantum signals cannot be amplified or copied accord-

ing to the well-known quantum no-cloning theorem (Wootters and Zurek, 1982). However, it is indeed possible to send quantum signals over arbitrary distances using a more complex communication protocol known as a quantum repeater (Briegel *et al.*, 1998). Here a quantum entangled state is repeatedly purified over a distance through the introduction of a network of intermediately located quantum nodes with extra quantum bits (Bennett *et al.*, 1996). Purified quantum entangled states of the network can then be used for quantum cryptography (Gisin *et al.*, 2002) or for faithful transmission of quantum signals over long distances through the quantum teleportation protocol (Bennett *et al.*, 1993).

Quantum networks can be divided into two major classes: (1) quantum communication networks for the transmission of quantum information, perhaps over long distances with quantum repeater circuitry; and (2) quantum computation networks for the distribution of quantum entanglement over large numbers of quantum memories for large-scale quantum processing. A quantum repeater network is shown in Fig. 1(a), where the communication channel is broken into n segments with the communication distance of each segment within the signal attenuation length. One first establishes purified entangled states for each segment and then performs measurement on the intermediate nodes to connect the segments and obtain an entangled state over long distance, which can be used for subsequent transmission of quantum signals. A distributed quantum computation network is shown in Fig. 1(b), where local quantum processors, each with a small number of qubits, are wired together through photonic channels. This approach to quantum computing is compelling for physical platforms that excel for small quantum registers but cannot easily be scaled to large numbers of qubits. By connecting the small well-behaved quantum registers through photonic channels, one can increase the size of the system without limits, and allow scalable quantum computation. Future quantum networks may involve a combination of the above two prototypes, as it is desirable to have both long communication distances and large computational sizes.

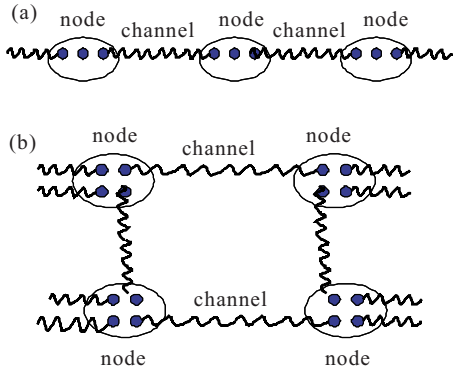

FIG. 1. (Color online) Illustration of different quantum networks. (a) Illustration of a quantum repeater network to extend the communication distance. (b) Illustration of a quantum computation network with many interconnected quantum nodes to extend the computational size.

B. Probabilistic versus deterministic approaches to quantum networks

Quantum communication channels are naturally carried by photons. On the other hand, quantum nodes are best implemented with material qubits to provide long storage times for quantum information. For instance, the hyperfine levels of the atoms (neutral or charged) have long coherence times and are a good choice of the stationary qubits at the quantum nodes. To realize a quantum network, we must coherently transfer quantum information from the stationary matter qubits to the flying photon qubits. There are two methods to achieve coherent information transfer between material and photonic qubits. The deterministic approach relies on high-quality optical resonators (cavities) to achieve the strong-coupling condition (Cirac *et al.*, 1997), and scaling to larger entangled networks is straightforward in principle but difficult in practice. The probabilistic approach (Duan *et al.*, 2001; Duan and Monroe, 2007) does not require strong-coupling cavities (although cavities are still helpful to boost up the coupling efficiency) and is more robust to noise. However, probabilistic protocols rely on special error-correction protocols with a certain overhead in qubits and time to achieve efficient scaling to large-scale networks.

When an optically active material qubit is excited with a laser, it normally couples to an infinite number of optical vacuum modes throughout the entire emission solid angle. The coherent transfer of quantum information requires a particular optical mode to be selected as the photonic qubit, and coupling of the material qubit to all other modes must be suppressed. In the deterministic approach, this selection is achieved through a high-quality cavity which enhances the coupling to the desired cavity mode (Kimble, 2008). The residual coupling to the other optical vacuum modes in free space can be considered spontaneous emission noise. For a high signal-to-noise ratio, we require the condition $C \equiv g^2/\kappa\gamma \gg 1$, where g is the coupling rate of the material qubit to the cavity mode, κ is the cavity decay rate, and γ is the spontaneous emission rate. The ratio $1/C$ is a measure of the fraction of the light entering the wrong modes and thus characterizes the fidelity error of a deterministic quantum operation. In the probabilistic approach, the detection of photons in the scheme allows us to know when the emitted photon has entered the correct mode. This built-in photon detection thus trades fidelity error in the deterministic approach to a lower efficiency (success probability less than unity) in the probabilistic scheme. However, when the operation succeeds, this lower efficiency has no influence on the resulting fidelity. This efficiency error is therefore heralded, which allows scaling methods that can tolerate very high efficiency errors (very low success probabilities) (Duan *et al.*, 2001; Duan and Monroe, 2007). Because of this inherent error detection, the probabilistic schemes are in general more robust to noise compared with the deterministic schemes. In this Colloquium, we

focus on the probabilistic approach to quantum networking which has inherent robustness to the dominant sources of noise in real experiments.

C. Physical systems for implementation of quantum networks

While the most natural platform of a quantum communication channel is photons, the quantum nodes can be implemented with various material systems, given that the coherence time of the quantum memory is sufficiently long. Atomic systems are particularly well-behaved quantum nodes with quantum information stored, for example, in different hyperfine levels within the ground-state manifold of the atoms, as in microwave atomic clocks.

Two well-studied approaches for atomic qubits are atomic ensembles and single atoms. Following the so-called Duan-Lukin-Cirac-Zoller (DLCZ) scheme (Duan *et al.*, 2001), atomic ensembles are widely considered as quantum nodes for quantum communication and quantum repeater networks. Here quantum information is stored in a collective excitonic state of an ensemble of atoms, and due to the interference of the photon emission from different atoms, this collective atomic state couples primarily to photon modes propagating in particular directions (Duan *et al.*, 2002). The resulting collective enhancement effect can be exploited to dramatically improve the coherent coupling between the collective atomic qubit and the photonic qubit. In recent years, remarkable experimental progress has been achieved along these lines, and we refer to a recent review for a detailed account on this approach and a comprehensive list of references (Kimble, 2008). The coherence (storage) time in atomic ensemble qubits is mainly limited by inhomogeneous magnetic fields throughout the atomic sample to the microsecond time scale (Kuzmich *et al.*, 2003). By switching off external magnetic fields and exploiting the atomic Mott insulator phase in a three-dimensional far-tuned optical lattice, longer coherence times up to hundreds of milliseconds have been achieved recently (Schnorrberger *et al.*, 2009). For this ensemble approach, although experiments are primarily based on clouds of neutral atoms, it is conceivable that other ensembles of particles could work equally well given long enough coherence times. For instance, there have been proposals for using ensembles of impurities in solids or quantum dots for implementation of quantum nodes (Staudt *et al.*, 2007).

Single atoms (charged or neutral) can also be used to implement the quantum nodes. We consider, in particular, single atomic ions as their additional charge degree of freedom allows them to be trapped easily for a long time. For single emitters, there is no collective enhancement effect for the light-atom coupling, so the connection efficiency of two segments of entanglement is typically much smaller compared with that of atomic ensembles. However, single atomic ions offer their particular advantages. First, single ions can be easily confined with internal-state-independent traps for weeks or longer, which allows a much longer operation time. The magnetic field insensitive "clock" states in trapped ions provide a particularly clean realization of a quantum memory, where coherence times of a few seconds are routine and can even approach the hour time scale (Bollinger *et al.*, 1991). Second, atomic qubits within trapped ions can be detected with near-unit detection efficiency through optical cycling transitions (Blatt and Zoller, 1988). Finally, unlike atomic ensembles, single atomic ions can be used for both quantum computation and communication networks (Duan *et al.*, 2004, 2006). We also note that trapped ions remain as one of the leading candidate hardwares for quantum computation based on local gates through their Coulomb-coupled motion (Cirac and Zoller, 1995; Blatt and Wineland, 2008). Therefore, the coupling of trapped ions to flying photonic qubits provides an interface between computation and communication qubits. A compelling possibility is a hybrid network that uses both the photonic coupling and the local Coulomb interaction. With trapped ions, the connection of various entangled segments can be achieved with local deterministic Coulomb-based gates instead of the probabilistic photon coupling, which could offer a more efficient network.

In this Colloquium, we focus on the use of trapped ions as quantum nodes, although some of the control schemes and the theoretical scaling methods discussed here can be readily applied to other experimental systems. In Sec. II, we review the recent experimental progress on protocols for trapped ion photonic quantum networking. In Sec. III, we detail scaling issues in ion or photon probabilistic networks in the context of long-distance quantum communication and large-scale quantum computation. Section IV concludes with a future outlook in photonic networks based on ions and other matter qubits.

II. TRAPPED ION QUANTUM NETWORK EXPERIMENTS

Trapped ions can be entangled through photonic networks using a variety of quantum optical techniques (Cirac *et al.*, 1997; Cabrillo *et al.*, 1999; Duan *et al.*, 2004; Moehring, Madsen, *et al.*, 2007). Current experiments follow the probabilistic protocols that offer more robustness to noise (Duan *et al.*, 2004; Moehring, Madsen, *et al.*, 2007). Typically, two ions are linked by first entangling the qubit state in each ion (denoted by $|0\rangle$ and $|1\rangle$) with an attribute of a photon and then coupling the two photons on a beam splitter or other interference element. An appropriate detection event following the interference "heralds" the entanglement of the parent atomic ions. Such a coupling is inherently probabilistic, limited in practice by finite photon detector efficiencies, optical losses, and inefficiencies in photon generation and collection. These losses and inefficiencies are characterized by the single parameter p, the success probability of linking or entangling the two ions.

We denote a type-I coupling as that involving a single photon between two ions and a type-II coupling involving two photons, one from each ion (Duan *et al.*, 2004). In a type-I link, the photon interference is between two

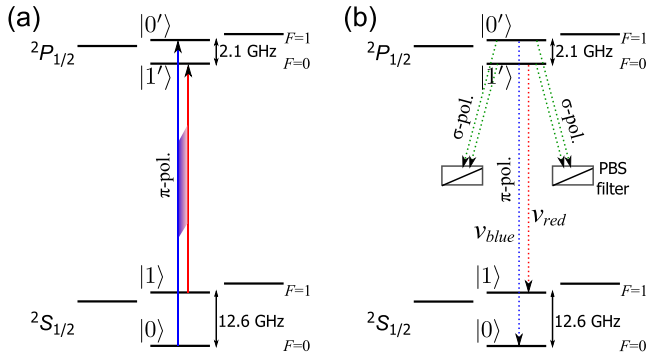

FIG. 2. (Color online) Reduced energy-level diagram of $^{171}Yb^+$, showing how photons are generated and entangled with internal ion qubits denoted by $|0\rangle$ and $|1\rangle$. (a) Due to the atomic selection rules, an ultrafast π-polarized laser pulse drives $|0\rangle$ to $|0'\rangle$ and $|1\rangle$ to $|1'\rangle$. The pulse bandwidth is large enough to simultaneously drive both transitions with near-unit excitation probability. (b) After excitation, the ion spontaneously decays back to $^2S_{1/2}$ and emits a single photon at 369.53 nm. If we consider only π-polarized photons, then the frequency of the emitted photon is entangled with the internal electronic state of the atom, with the separation of the different frequency modes equal to the sum of the $^2S_{1/2}$ and $^2P_{1/2}$ hyperfine splittings ($\nu_{blue}-\nu_{red}=14.7$ GHz). Polarizing beam splitters (PBS) are used to filter out the σ-polarized light.

possible paths of a single photon, and the differential optical phase of the two paths is imprinted onto the two-ion entangled state (Cabrillo *et al.*, 1999). A type-I link thus requires high mechanical stability of all optical paths to much better than an optical wavelength and also requires the ions to be confined sufficiently strong so that neither ion recoils in the absorption or emission process. However, the type-I photonic link offers the advantage of higher success probabilities since just a single photon is emitted and collected by the ion pair. Type-I interference between two ions has been observed between two ions held in the same trap (Eichmann *et al.*, 1993; DeVoe and Brewer, 1996). Type-II links have the advantage of being less sensitive to mechanical vibrations and alignment, and because ion or photon entanglement experiments primarily used this method, we limit the discussion in this Colloquium to such two-photon links between ions.

We concentrate on the $^{171}Yb^+$ atomic system (Balzer *et al.*, 2006; Olmschenk *et al.*, 2007), following ion or photon experiments, but there are other satisfactory atomic ion candidates for this purpose. Figure 2 shows a reduced energy-level structure of $^{171}Yb^+$, highlighting the $^2S_{1/2}$ ground-state qubit in the ($F=0$, $m_F=0$) and ($F=1$, $m_F=1$) hyperfine levels, denoted by $|0\rangle$ and $|1\rangle$, respectively, and separated in frequency by a hyperfine splitting of 12.643 GHz. Single qubit rotations can be accomplished with either resonant microwaves at this frequency or through optically stimulated Raman transitions through an excited ^2P state. Measurement of the $^{171}Yb^+$ qubit is accomplished through standard state-dependent fluorescence techniques (Blatt and Zoller, 1988) with effective qubit detection efficiencies greater than 98%.

A. Atom-photon entanglement

The simplest quantum link between trapped ion and photonic qubits follows from a resonant interaction between the ion and the photon (Blinov *et al.*, 2004; Moehring *et al.*, 2004). In Fig. 2, an ultrafast laser drives the $^2S_{1/2}\rightarrow{}^2P_{1/2}$ electronic transition near 369.53 nm. When the bandwidth of the laser pulse is large enough, both $|0\rangle\rightarrow|0'\rangle$ and $|1\rangle\rightarrow|1'\rangle$ transitions are driven simultaneously, where $|0'\rangle$ and $|1'\rangle$ refer to the $^2P_{1/2}$ ($F'=1$, $m'_F=0$) and ($F'=0$, $m'_F=0$) excited states, respectively. Given the angular-momentum selection rules and a laser that is linearly polarized along the quantization axis to drive $\Delta m=0$ transitions only, the qubit is mapped from the ground state to the excited state, as shown in Fig. 2(a). Following spontaneous emission (natural lifetime of $\tau\sim 8$ ns for the $^2P_{1/2}$ states) and conditioned upon the photon having been collected and successfully passed through a polarizing filter that rejects $\sigma_\pm$ polarizations, an ion initially prepared in the state $\alpha|0\rangle+\beta|1\rangle$ evolves to the postselected entangled state $\alpha|0\rangle|\nu_{blue}\rangle+\beta|1\rangle|\nu_{red}\rangle$, as shown in Fig. 2(b). Here the photonic qubit is stored in its frequency, with $|\nu_{blue}\rangle$ and $|\nu_{red}\rangle$ denoting the frequency-resolved states of the single photon (Madsen *et al.*, 2006). [In the $^{171}Yb^+$ ion, $\nu_{blue}-\nu_{red}=14.7$ GHz, while the bandwidth of either color photon is given by the excited-state linewidth $\gamma=1/\tau=(2\pi)20$ MHz; so these photon frequencies are well resolved.]

B. Two-photon interference

The central effect that will allow the ion qubits to be linked through photons is the phenomenon of two-photon quantum interference. When two photons interact on a beam splitter (BS), there are four possible outcomes, with each photon being either reflected or transmitted, as shown in Fig. 3. When the photons are identical in polarization and color, the outcomes of the photons emerging along different paths of a 50/50 BS will interfere destructively [Figs. 3(d) and 3(e)].

This two-photon interference effect can also be seen by considering the unitary operation of the BS on the photons in the two modes a and b depicted in Fig. 3. Given n and m photons in respective modes a and b before the BS, the action of the BS is identical to rotations within an effective $J=N/2$ angular-momentum system, where $N=n+m$. Formally, the two-mode input state $|n\rangle_a|m\rangle_b$ evolves to $|n\rangle_a|m\rangle_b\rightarrow e^{-i\chi\hat{J}_y}|n\rangle_a|m\rangle_b$, where the rotation angle χ is π times the reflectivity R of the lossless BS and $\hat{J}_y=-i(\hat{a}^\dagger\hat{b}-\hat{a}\hat{b}^\dagger)/2$ (Yurke *et al.*, 1986). The photon annihilation and creation operators, $\hat{a}$ and $\hat{a}^\dagger$ for mode a and $\hat{b}$ and $\hat{b}^\dagger$ for mode b, follow the usual bosonic commutation relations $[\hat{a},\hat{a}^\dagger]=[\hat{b},\hat{b}^\dagger]=1$. For

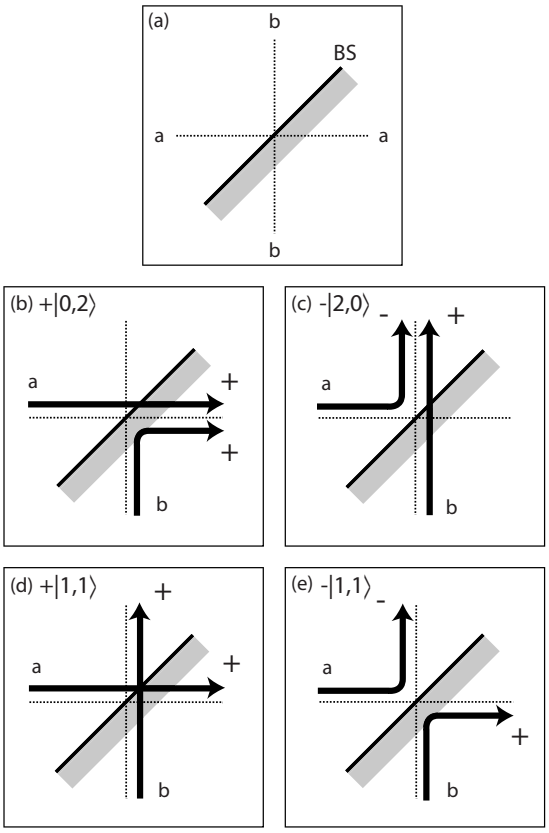

FIG. 3. Two photon interference at a beam splitter. (a) Spatial modes a and b are straight paths through the beam splitter (BS), and the beam splitter couples these two modes. (b)–(e) The four possible output modes of two photons entering a beam splitter from different ports. A negative phase is acquired only upon reflection from low to high index of refraction—mode a in (c) and (e).

one photon initially in both modes ($N=2$), we find that

$$|1\rangle_a|1\rangle_b \rightarrow \frac{1}{\sqrt{2}}\sin\chi|2\rangle_a|0\rangle_b + \cos\chi|1\rangle_a|1\rangle_b - \frac{1}{\sqrt{2}}\sin\chi|0\rangle_a|2\rangle_b, \quad (1)$$

and for a 50/50 BS ($\chi=\pi/2$), the $|1\rangle_a|1\rangle_b$ output state vanishes.

Two-photon quantum interference has been observed in nonlinear down-conversion of photons (Hong *et al.*, 1987; Shih and Alley, 1988; Kaltenbaek *et al.*, 2006), quantum dots (Santori *et al.*, 2002), single atoms (Legero *et al.*, 2004; Beugnon *et al.*, 2006), atomic ensembles (Felinto *et al.*, 2006; Thompson *et al.*, 2006; Chaneliere *et al.*, 2007), and trapped ions (Maunz *et al.*, 2007; Gerber *et al.*, 2009).

In the $^{171}Yb^+$ system, two-photon quantum interference is observed by simultaneously exciting two trapped $^{171}Yb^+$ ions, combining the two emitted photons on the beam splitter, and detecting the photons with a photomultiplier tube (PMT) at each of the two output ports of the beam splitter. The joint probability of detection for identical photons is measured by placing matched polarizers in each beam path, while detection of distinguishable photons is evaluated by including the $\lambda/2$ waveplate in one of the two input paths to the beam splitter. As shown above, for identical photons we expect no detections at time delay $t_d=0$, while for distinguishable photons we expect a probability of joint detection half as large as that from adjacent excitations from the laser-pulse train. The data shown in Fig. 4 demonstrate this quantum two-photon interference effect. In the measurement of parallel polarized photons, the residual counts at time delay $t_d=0$ result from both dark counts on the PMTs and imperfect spatial mode overlap of the photons on the beam splitter. The data shown in Fig. 4 correspond to an interferometer contrast of approximately 95% (Maunz *et al.*, 2007). The spatial filtering afforded by coupling the spontaneously emitted photons into single-mode fibers is essential to achieving such levels of two-photon interference.

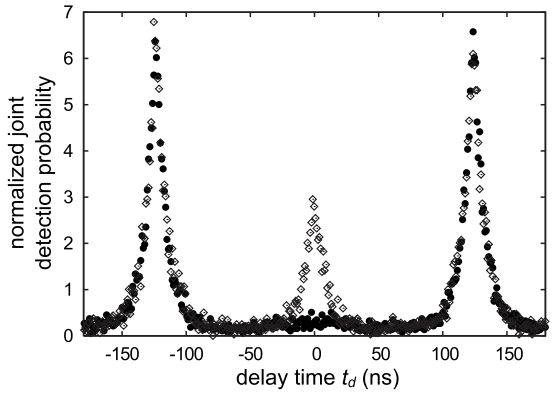

FIG. 4. Normalized experimental two-photon second-order correlation function for identical (parallel polarized) photons (diamonds) and distinguishable (perpendicularly polarized) photons (circles) (Maunz *et al.*, 2007). As expected, two identical photons incident on the beam splitter always exit by the same port, resulting in suppression of joint detections at time delay $t_d=0$.

C. Ion-ion entanglement

Two ions become entangled by coupling the two photons on a beam splitter and measuring an appropriate coincident event on detectors behind the beam splitter, as shown in Fig. 5 (Moehring, Maunz, *et al.*, 2007; Matsukevich *et al.*, 2008; Maunz *et al.*, 2009; Olmschenk *et al.*, 2009). For two independent ions A and B, initially prepared in unique qubit states $\alpha|0\rangle_A+\beta|1\rangle_B$ and $\gamma|0\rangle_A+\delta|1\rangle_B$, synchronized laser pulses can simultaneously promote both ions to their excited states, and given that a single photon is emitted from each ion, collected into a single spatial mode, and passed through polarizing filters, the postselected state of this four-qubit system is

$$|\psi\rangle_{AB} = (\alpha|0\rangle_A|\nu_{\text{blue}}\rangle_A + \beta|1\rangle_A|\nu_{\text{red}}\rangle_A) \otimes (\gamma|0\rangle_B|\nu_{\text{blue}}\rangle_B + \delta|1\rangle_B|\nu_{\text{red}}\rangle_B). \quad (2)$$

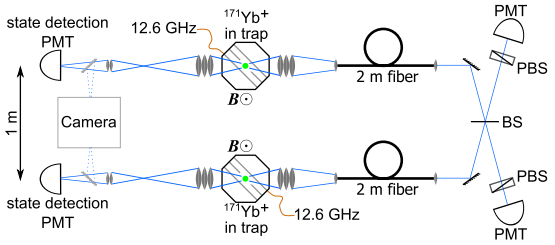

FIG. 5. (Color online) Experimental setup for the heralded entanglement and quantum gate operation between two ions. Spontaneously emitted π-polarized photons are coupled in a single-mode fiber and directed to interfere on a 50/50 nonpolarizing BS. Coincident detection of two photons by photon-counting photomultipliers (PMTs) announces the success of the gate between the two ions. PBSs are polarizers used to filter the photons so that only π-polarized photons are detected. The state of each ion is measured by state-dependent fluorescence, detected by a PMT on the opposite side of the vacuum chamber.

As described above, when the two spatial modes A and B of the photons are matched on a 50/50 beam splitter, the components of the above state with photons of identical color result in the photons emerging from the beam splitter (Hong *et al.*, 1987; Shih and Alley, 1988), and it is only the case of different color photons that result in photons emerging the beam splitter along different spatial modes. Thus when photons are detected in coincidence on the two detectors, the ions are projected onto the general entangled state (Braunstein and Mann, 1995),

$$|\psi\rangle_{AB} = \alpha\delta|0\rangle_A|1\rangle_B - \beta\gamma|1\rangle_A|0\rangle_B. \tag{3}$$

We first assess the generation of the maximally entangled antisymmetric Bell state $(|0\rangle_A|1\rangle_B - |1\rangle_A|0\rangle_B)$ by setting $\alpha=\beta=\gamma=\delta$ and performing quantum tomography on the resulting state. The resulting density matrix ρ shown in Fig. 6 is obtained using a maximum-likelihood method from an overcomplete set of measurements of the two spins in various bases (James *et al.*, 2001). The entanglement of the resultant state ρ can be characterized with either the entanglement fidelity or the entanglement of formation (or equivalently the concurrence) (Wootters, 1998). The entanglement fidelity is defined as the overlap with a maximally entangled state $|\psi_e\rangle=(|0\rangle_A|1\rangle_B-|1\rangle_A|0\rangle_B)/\sqrt{2}$ as $\mathcal{F}=\langle\psi_e|\rho|\psi_e\rangle$. A fidelity $\mathcal{F}>1/2$ shows that the state ρ is entangled (Sackett *et al.*, 2000). Given the measured quantum state ρ, the concurrence $\mathcal{C}$ and the entanglement of formation E_F can also be calculated (Wootters, 1998), with $\mathcal{C}>0$ or $E_F>0$ indicating entanglement. From the measured data, we calculate an entanglement fidelity of $\mathcal{F}=0.87(2)$, a concurrence of $\mathcal{C}=0.77(4)$, and an entanglement of formation $E_F=0.69(6)$ (52).

In general, the overall action of the photon heralding process resulting in the evolution from Eqs. (2) to (3) is a probabilistic quantum gate where the input state $|\Psi_{\text{in}}\rangle$ is transformed to

$$|\Psi_{\text{out}}\rangle \propto Z_1(I - Z_1Z_2)|\Psi_{\text{in}}\rangle, \tag{4}$$

with success probability p, where Z_i is the Pauli Z operator on ion i. This type of gate was recently demonstrated with a fidelity of approximately 90% averaged over a replete set of quantum states on the Bloch sphere (Maunz *et al.*, 2009).

The above probabilistic gate can also be exploited to teleport the state of one ion to the other, as shown in Fig. 7. Here the gate is operated with $\gamma=\delta=1/\sqrt{2}$, and the state of ion A represented by the amplitudes α and β is teleported to ion B by measuring ion A following a

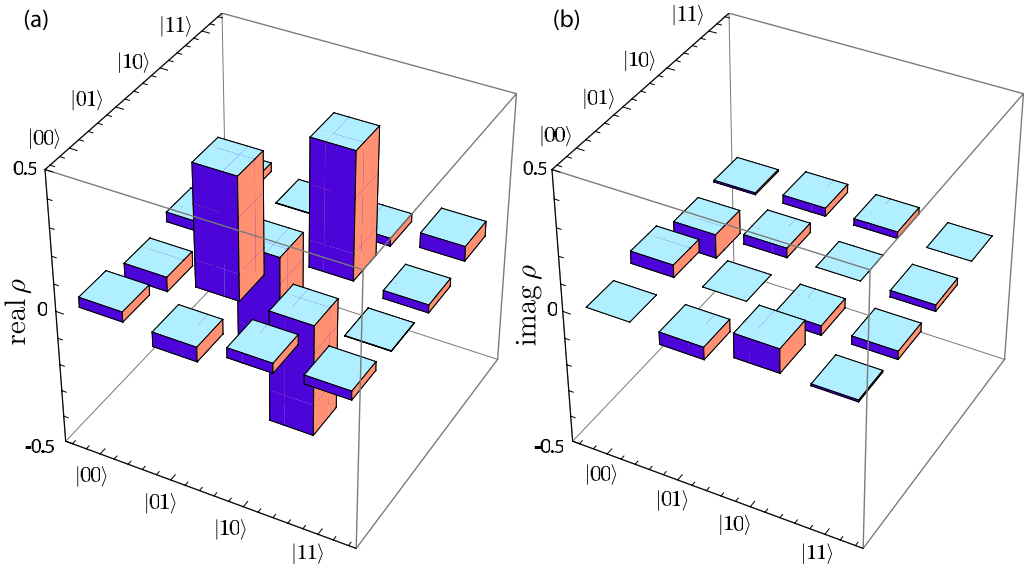

FIG. 6. (Color online) State tomography of the singlet entangled state of two ions $|0\rangle|1\rangle-|1\rangle|0\rangle$. The (a) real and (b) imaginary elements of the reconstructed density matrix are shown. The density matrix was obtained with a maximum-likelihood method from 601 events measured in nine different bases. From this density matrix we calculate an entangled state fidelity of $\mathcal{F}=0.87(2)$, a concurrence of $C=0.77(4)$, and an entanglement of formation $E_F=0.69(6)$.

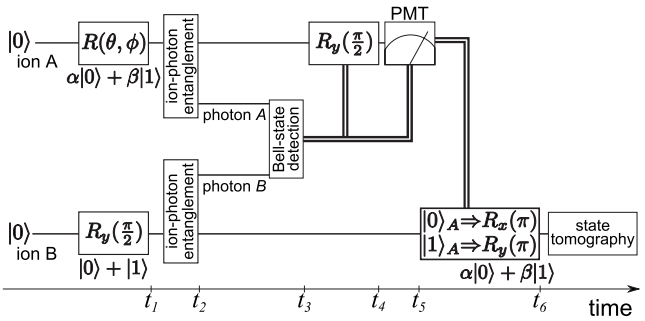

FIG. 7. Space-time schematic of the teleportation protocol. Each ion is first initialized to $|0\rangle$ by optical pumping. At time t_1 the state to be teleported $\alpha|0\rangle+\beta|1\rangle$ is written to ion A and the known state $|0\rangle+|1\rangle$ is written to ion B through appropriate rotation operators $R(\theta,\phi)$ on the Bloch sphere, with $R(\theta,0) \equiv R_y(\theta)$ and $R(\theta,\pi/2) \equiv R_x(\theta)$. At time t_2, synchronized laser pulses excite each atom, and the frequencies of the emitted photons are entangled with the respective ion qubits following Fig. 2. The two photons interfere at a beam splitter, and coincident detection of the emerging photons at time t_3 heralds the production of the entangled state of Eq. (3) with $\delta=\gamma=1/\sqrt{2}$. Following successful entanglement, ion A is coherently rotated at time t_4 through the operator $R_y(\pi/2)$ and measured in the z-basis at time t_5. Finally, depending on the measurement result, rotation operators conditioned upon the measurement result are applied to ion B at time t_6 to complete the teleportation of the original quantum state from A to B.

$\pi/2$ rotation of its qubit. Based on this measurement, an appropriate rotation is then applied to ion B, thus recovering the original qubit on ion B. This probabilistic teleportation protocol was implemented on a pair of $^{171}Yb^+$ ions separated by $\sim$1 m, with an averaged fidelity of 90% (Olmschenk *et al.*, 2009). Figure 8 shows the tomographically measured density matrices of six teleported states distributed on the Bloch sphere, with the input states listed below each entry.

D. Errors and success probabilities

The observed remote ion-ion entanglement and teleportation fidelities are consistent with known experimental errors. The primary contributions to the error are imperfect state detection (3%), spatial mode mismatch on the beam splitter (6%), and detection of σ-polarized light due to the finite solid angle of collection and misalignment of the magnetic field ($<2\%$). Other sources, including imperfect state preparation, pulsed excitation to the wrong atomic state, dark counts of the PMT leading to false coincidence events, and multiple excitation due to pulsed laser light leakage, are each estimated to contribute to the overall error by much less than 1%. Micromotion at the rf-drive frequency of the ion trap, which alters the spectrum of the emitted photons and can degrade the quantum interfer-

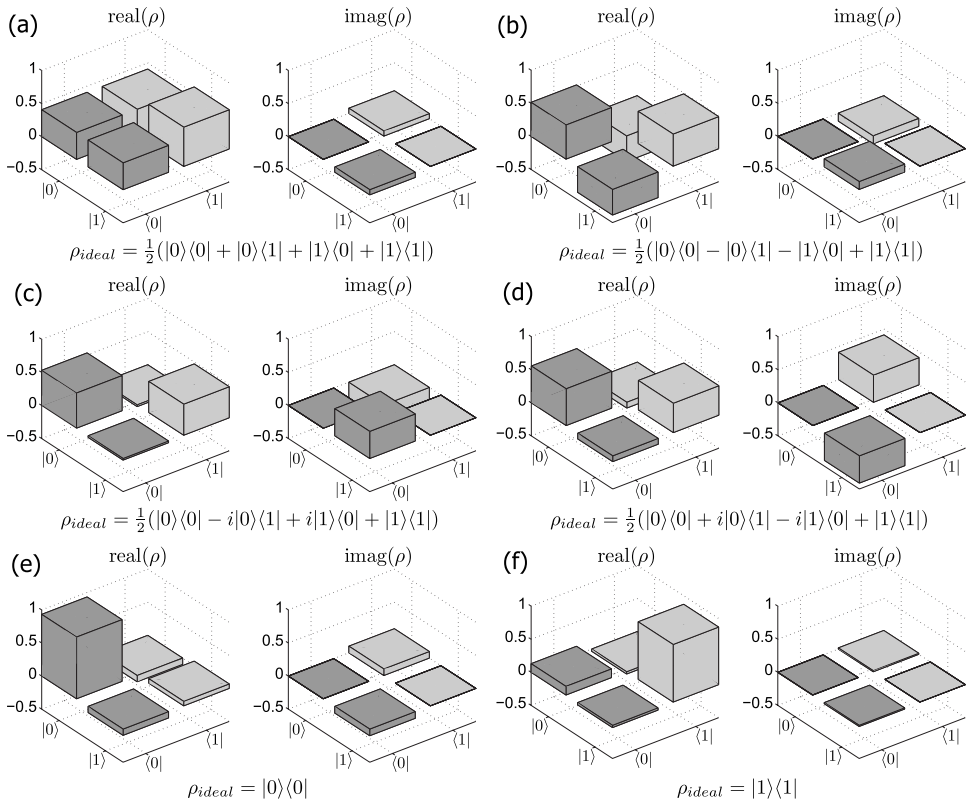

FIG. 8. Tomography of the teleported quantum states. The reconstructed density matrices ρ for the six unbiased basis states teleported from ion A to ion B: (a) $|\psi\rangle_{\text{ideal}}=1/\sqrt{2}(|0\rangle+|1\rangle)$ teleported with fidelity $\mathcal{F}=0.91(3)$, (b) $|\psi\rangle_{\text{ideal}}=1/\sqrt{2}(|0\rangle-|1\rangle)$ teleported with fidelity $\mathcal{F}=0.88(4)$, (c) $|\psi\rangle_{\text{ideal}}=1/\sqrt{2}(|0\rangle+i|1\rangle)$ teleported with fidelity $\mathcal{F}=0.92(4)$, (d) $|\psi\rangle_{\text{ideal}}=1/\sqrt{2}(|0\rangle-i|1\rangle)$ teleported with fidelity $\mathcal{F}=0.91(4)$, (e) $|\psi\rangle_{\text{ideal}}=|0\rangle$ teleported with fidelity $\mathcal{F}=0.93(4)$, and (f) $|\psi\rangle_{\text{ideal}}=|1\rangle$ teleported with fidelity $\mathcal{F}=0.88(4)$. These measurements yield an average teleportation fidelity $\overline{\mathcal{F}}=0.90(2)$. The data shown comprise a total of 1285 events in 253 h.

ence, is expected to contribute to the overall error by less than 1%.

This quantum linkage is a heralded probabilistic process. The net probability p for the success of the gate operation in the experiments is

$$p = \tfrac{1}{4}[p_\pi \eta T_{\text{fiber}} T_{\text{optics}} \xi \eta_c]^2 \approx 2.2 \times 10^{-8}, \quad (5)$$

where $p_\pi = 0.5$ is the fraction of photons with the correct polarization (half are filtered out as being produced by σ decays), $\eta = 0.15$ is the quantum efficiency of each PMT, $T_{\text{fiber}} = 0.2$ is the coupling and transmission of each photon through the single-mode optical fiber, $T_{\text{optics}} = 0.95$ is the transmission of each photon through the other optical components, $\xi = 1 - 0.005 = 0.995$, with 0.005 the branching ratio from the $2P_{1/2}$ state to the $^2D_{3/2}$ level, and $\eta_c = 0.02$ is the collection efficiency of the photons, given by the solid angle of the collection optics.

In the above experiments, the attempt rate was limited to about 75 kHz due to the time required for the initial microwave pulse for state preparation. This resulted in about one successful gate operation every 12 min. However, the expression for the success probability p reveals multiple ways to substantially increase the success rate. The most dramatic improvement would be to increase the effective solid angle of collection, which, for instance, could be accomplished with high numerical aperture optics or by surrounding each ion with an optical cavity. In the latter case, the collection efficiency can be as high as $\eta_c \sim 2C/(1+2C)$ (Luo *et al.*, 2009), where $C = g^2/\kappa\gamma$ is the single-atom cooperativity parameter; g is the ion-cavity coupling rate, κ is the cavity decay rate, and γ is the ion spontaneous emission rate. For a cavity in the intermediate coupling region with $C \sim 1$, the collection efficiency can be improved to $\eta_c \sim 67\%$. In addition, photons emerging from a cavity mode will efficiently couple to a single-mode fiber (coupling efficiencies of $T_{\text{fiber}} \sim 90\%$ have been achieved in many experiments). The use of such a cavity could thus increase the gate success probability by a factor of $\sim 10^5$ over current experiments. The detection efficiency η can be improved substantially with specialized solid-state or superconducting photon detectors (Miller *et al.*, 2003), although speed and dark-count parameters must also be considered. Finally, the prefactor 1/4 appearing in the success probability of Eq. (5) can be improved to 1/2 by resolving the frequency components behind each arm of the beam splitter and detecting appropriate coincident events with four PMTs (Braunstein and Mann, 1995; Michler *et al.*, 1996). Considering all of these improvements, it may be possible in the future to reach gate success probabilities of $p > 10^{-2}$. Such experimental improvements would dramatically impact the scalability of probabilistic ion or photon networks.

III. THEORETICAL SCALING TOWARD LARGE-SCALE QUANTUM NETWORKS

From Sec. II, we see that a number of basic steps for trapped ion photonic quantum networks have been demonstrated in small systems consisting of a few qubits. In this section, we review several methods to scale the current experimental system toward realization of large quantum networks. In Sec. III.A, we show how to realize a quantum repeater network based on probabilistic entanglement between remote ions. Second, we show that a telequantum-computational network can be realized in an efficient fashion exclusively with probabilistic gate operations even when the gate success probability is well below unity. Third, we review a hybrid approach toward large-scale quantum networks especially suited to trapped ion qubits, where both local deterministic gates and remote probabilistic entanglement are used. This hybrid approach exhibits a more favorable scaling law and thus allows even smaller gate success probabilities ($p \ll 1$). Given the availability of local deterministic gates for the trapped ions through the Coulomb interaction, this hybrid approach may offer a more practical method for building future networks of large sizes.

A. An extension of the DLCZ scheme for the quantum repeater network with trapped ions

The DLCZ scheme for the implementation of a quantum repeater network was initially designed with atomic ensembles as the quantum nodes (Duan *et al.*, 2001). There are two key features of this scheme: first is a particular interaction configuration between light and atoms that entangles a photon with a collective mode in the atomic ensemble. This involves a collective enhancement of the interaction that substantially increases the signal-to-noise ratio but because this is unique to a particle ensemble system it does not carry over to single-particle nodes. The second feature of the DLCZ scheme is its inherent insensitivity to the dominant source of experimental noise in practical experimental systems. As opposed to the original quantum repeater protocol (Briegel *et al.*, 1998), where every source of noise must have a level below an error threshold of approximately a few percent, the DLCZ scheme can tolerate very high levels of photon loss. (However, other sources of noise such as detector dark counts must still be below more strict error thresholds.) In atomic ensembles, photon loss occurs with a probability typically greater than 50%, yet can still be efficiently scaled to large communication distances.

We can readily extend the DLCZ scheme for a quantum repeater network to single particles (single trapped ions here) as the quantum nodes while maintaining the insensitivity to the dominant source of noise. As shown in Sec. II, one can generate entanglement between remote ions, with a success probability p, encompassing all sources of photon losses, from finite collection solid angle, fiber coupling, absorption, and finite detector efficiencies. Using the same light-atom interaction interface, one can also connect two segments of entanglement to double the communication distance as shown in Fig. 9. The success probability for the entanglement connection, denoted by p_c, can be somewhat higher than p as the entanglement connection operation applies to two

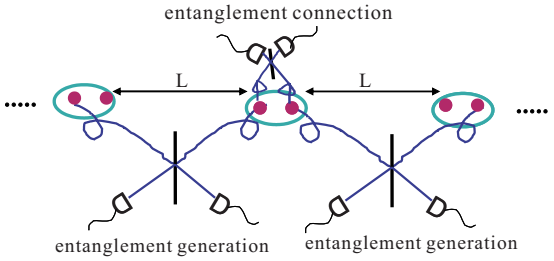

FIG. 9. (Color online) Illustration of construction of a quantum repeater network through probabilistic entangling operations.

local ions and can thus avoid photon loss in the communication channel. For each step of the connection, the communication distance L is doubled, so the recursion relation for L is $L_i=2L_{i-1}$ for the ith step. The connection succeeds with a probability p_c, so we need in average to repeat the connection $1/p_c$ times for a successful event. The recursion relation for the preparation time is given by $T_i\sim(1/p_c)T_{i-1}$. Combining these two recursion relations, we obtain the scaling

$$T\sim T_0(L/L_0)^{\log_2(1/p_c)}, \tag{6}$$

where $T_0\sim t_a/p$ is the preparation time of entanglement over an initial segment of length L_0, with t_a denoting the time for each entangling attempt. With ensembles, the scaling is instead given by

$$T\sim T_0(L/L_0)^{(1/2)\log_2(L/L_0)+\log_2(1/p_c-1)+5/2}$$

(Duan *et al.*, 2001). The additional factor $(1/2)\log_2(L/L_0)+5/2$ in the exponent arises from the postselection in each step necessary to eliminate double excitations in the ensemble. With single ions, however, there are no double excitations and thus no postselection (although it is still probabilistic). This is the key advantage of using single ions as repeater nodes. The price for this more favorable scaling is that the connection efficiency p_c is typically much smaller for single ions compared with atomic ensembles because there is no collective enhancement effect for single particles. Although the scaling given above is a polynomial in both the distance L and the inverse of the success probability $1/p_c$, the success probability p_c should not be too low to have a practical scaling exponent (a value of a few percent appears tolerable). Such a success probability will require special optical elements such as an optical cavity or high numerical aperture optics, as discussed in Sec. II.D. Alternatively, one can apply local deterministic gates to adjacent ions to connect different segments of ion entanglement as covered below.

B. Quantum computational network with exclusively probabilistic quantum gates

As discussed in Sec. II, with an appropriate laser-ion interaction configuration, we can realize probabilistic quantum gates on remote ions (Duan *et al.*, 2006; Maunz *et al.*, 2009). As a gate keeps track of information of the input states, it is more powerful than a probabilistic entangling operation. With entangling operations, we can establish entangled states over long distance associated with the quantum repeater network; with probabilistic gate operations, we can realize a fully functional quantum computation network, which allows generation of any entangled states distributed over many remote parties. Similar to the probabilistic entangling operations, the probabilistic gates are inherently robust to noise in the sense that the dominant noise in the experimental system represented by the photon loss only contributes to a finite probability of the gate failure and does not degrade the gate fidelity when it succeeds. Quantum computation with probabilistic gates thus tolerates this dominant noise at a much higher level. One can show that scalable quantum computation can be built up solely based on the probabilistic gates. Compared with the deterministic gates, the additional overhead (such as the number of qubit manipulations) for quantum computing with probabilistic gates scales only polynomially with both the size of the computation and the inverse of the gate success probability (Duan and Raussendorf, 2005; Lim *et al.*, 2006).

Here we explain how to build a quantum computational network with the probabilistic measurement gate, following the approach of Duan and Raussendorf (2005) and Duan *et al.* (2006). The probabilistic measurement gates on remote ions, reviewed in Sec. IV and realized recently in experiments (Maunz *et al.*, 2009; Olmschenk *et al.*, 2009), are based on the interference of photonic qubits stored in the frequency (color) of the photons. There are other proposals for the implementation of probabilistic gates using atomic qubits (Barrett and Kok, 2005; Duan *et al.*, 2005; Lim *et al.*, 2006). However, the probabilistic measurement gate of Duan *et al.* (2006) has several advantages in terms of experimental requirements:

- Optical frequency qubits are used to connect and entangle matter qubits at distant locations. The two states comprising this optical qubit have the same polarization but differ in frequency by the atomic hyperfine splitting (typically in the microwave region). These closely spaced frequency components have basically zero dispersion in typical optical paths; thus this optical qubit is highly insensitive to phase jitter inherent in optical interferometers.
- The gate scheme does not require interferometric stabilization of the optical path lengths to near or within an optical wavelength.
- The motion of the atomic qubits need not be confined to within an optical wavelength (the Lamb-Dicke regime).

As outlined in Sec. II, the probabilistic measurement gate projects the ion states to the eigenspace of the operator Z_1Z_2, where Z_i represents the Paul phase flip operator acting on the qubit states of the ith ion [Eq. (4)].

Various sources of noise in the experimental system lead to a finite (and typically small) gate success prob-

ability p. The single-bit operations can be done for single ions with a very high precision, so we neglect their error in the following. The probabilistic measurement gates, together with single-bit operations, are then enough for efficient construction of universal quantum computation. To prove this result, it is most convenient to use the cluster-state approach to quantum computation (Raussendorf and Briegel, 2001). In the cluster-state approach, universal quantum computation can be realized through a combination of single-bit operations together with the preparation of a particular many-body entangled state, which is typically chosen as the two-dimensional (2D) cluster state. In the ion system, as we get single-bit operations almost for free, our task reduces to how to efficiently construct a large-scale 2D cluster state with the probabilistic measurement gates. The construction of the 2D cluster state in the following is divided into two steps: first we show how to efficiently prepare a one-dimensional (1D) cluster state from the probabilistic measurement gates using the divide and conquer method and then we give a construction to efficiently generate 2D cluster states from the 1D chains.

With respect to a given lattice geometry, the cluster state is defined as coeigenstates of all operators $A_i = X_i \Pi_j Z_j$, where i denotes an arbitrary lattice site and j runs over all the nearest neighbors of the site i (Briegel and Raussendorf, 2001). X_i and Z_j denote the Pauli spin and the phase flip operators on the qubits at the sites i,j, respectively. One can easily check that all operators A_i commute with each other, and they are referred to as the stabilizer operators. The properties of the cluster state can be conveniently explained by studying the corresponding set of stabilizer operators. In our construction of lattice cluster states with probabilistic ZZ measurement gates, we make use of the following properties of the ZZ gate on the cluster states. (1) If one starts with two qubits (atoms) in a product state given by the coeigenstate of X_1 and X_2 (it is thus also an eigenstate of X_1X_2), after a ZZ measurement, the state is projected to an eigenstate of Z_1Z_2. As the measurement operator Z_1Z_2 commutes with X_1X_2, the final state is still an eigenstate of X_1X_2 (but not of X_1 and X_2 anymore). The state after measurement is thus a coeigenstate of the stabilizer operators Z_1Z_2 and X_1X_2, which is equivalent to the two-qubit cluster state under a single-bit rotation that exchanges Z_2 and X_2. (2) Assume that one has prepared two 1D cluster chains, each of n qubits. The stabilizer operators for the boundary qubits n and $n+1$ of the two chains are denoted by X_nZ_{n-1} and $X_{n+1}Z_{n+2}$, respectively. Similar to the argument in property (1), a ZZ measurement of these two boundary qubits generates the new stabilizer operators Z_nZ_{n+1} and $X_nX_{n+1}Z_{n-1}Z_{n+2}$ (the initial stabilizer operators X_nZ_{n-1} and $X_{n+1}Z_{n+2}$ are destroyed by the measurement, but their product $X_nX_{n+1}Z_{n-1}Z_{n+2}$ is preserved as it commutes with the measurement operator Z_nZ_{n+1}). This operation actually connects the two chains into a cluster state of $2n-1$ qubits. (The central qubits n and $n+1$ together represent one logic qubit with the encoded $X_L = X_nX_{n+1}$ and $Z_L = Z_n$ or Z_{n+1}. One can measure the single-bit operator X_{n+1} to reduce the encoded operators X_L and Z_L to X_n and Z_n.) (3) If we destroy the state of an end qubit of an n-qubit cluster chain, for instance, through an unsuccessful attempt of the ZZ measurement, we can remove this bad qubit by performing a Z measurement on its neighboring qubit and recover a cluster state of $n-2$ qubits. (4) We can shrink a cluster state by performing an even number of X measurements on the connecting qubits. The last two properties can be explained in a similar way by looking at the transformation of the set of stabilizer operators through the measurement, and the detailed explanation can be found in Hein *et al.* (2006). The above properties of the cluster states are shown in Fig. 10.

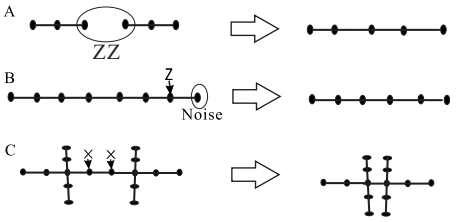

FIG. 10. Illustration of the three properties of the cluster states which are important for our construction of such states with the probabilistic entangling gates: (a) extend cluster states with ZZ measurement gates, (b) recover cluster states by removing bad qubits, and (c) shrink cluster states for more complicated links [see Duan and Raussendorf (2005)].

If we have generated two sufficiently long cluster chains each of n_0 qubits, we can try to connect them through a probabilistic ZZ gate. If this attempt fails, through property (2), we can recover two (n_0-2)-qubit cluster chains through a Z measurement and try to connect them again. As one continues with this process, the average number of qubits in the connected chain is then given by $n_1 = \Sigma_{i=0}^{n_0/2}(2n_0-1-4i)p(1-p)^i \simeq 2n_0-1-4(1-p)/p$, where the last approximation is valid when $e^{-n_0p/2} \ll 1$. As a result, the average chain length increases if $n_0 > n_c \equiv 4(1-p)/p+1$. We can iterate these connections to see how the computational overhead scales with the qubit number n. We measure the computational overhead in terms of the total computation time and the total number of attempts for the ZZ gates. For the rth $(r \geqslant 1)$ round of successful connection, the chain length n_r, the total preparation time T_r, and the total number of attempts M_r scale in a manner that can be obtained from the recursion relations $n_r \approx 2n_{r-1}-n_c$, $T_r \approx T_{r-1}+t_a/p$, and $M_r \approx 2M_{r-1}+1/p$, respectively. In writing the recursion relation for T_r, we have assumed that two cluster chains for each connection are prepared in parallel, and we neglect the time for single-bit operations (t_a denotes the time for each attempt of the ZZ gate). From the above recursion relations, we conclude that if we can prepare cluster chains of n_0 $(n_0 > n_c)$ qubits in time T_0 with M_0 attempts of the probabilistic gates, for a large cluster state, the preparation time T and the number of attempts M scale with the chain length n as $T(n) \approx T_0$

$+(t_a/p)\log_2[(n-n_c)/(n_0-n_c)]$ and $M(n)\approx(M_0+1/p)(n-n_c)/(n_0-n_c)-1/p$.

In the above we have shown that if one can prepare cluster chains longer than some critical length n_c, one can generate large-scale 1D cluster states very efficiently. The problem then reduces to how to efficiently prepare cluster chains up to the critical length n_c. If one wants to prepare an n-qubit cluster chain, we propose to use a repeater protocol which divides the task into $m=\log_2 n$ steps: for the ith ($i=1,2,\ldots,m$) step, we attempt to build a 2^i-bit cluster state by connecting two 2^{i-1}-bit cluster chains through a probabilistic ZZ gate. If such an attempt fails, we discard all qubits and restart from the beginning. For the ith step, the recursion relations for the preparation time T_i and the number of attempts M_i are given by $T_i\approx(1/p)(T_{i-1}+t_a)$ and $M_i\approx(1/p)(2M_{i-1}+1)$, which, together with $T_1\approx t_a/p$ and $M_1\approx 1/p$, give the scaling rules $T(n)\approx t_a(1/p)^{\log_2 n}$ and $M(n)\approx(2/p)^{\log_2 n}/2$. The cost is more significant, but it is still a polynomial function of n. The scaling in this repeater protocol compares favorably with the exponential scaling $T(n)\sim M(n)\sim(1/p)^{n-1}$ in the direct protocol, where to construct an n-qubit cluster chain one requires the $n-1$ ZZ gates to succeed simultaneously.

To generate a cluster chain of a length $n>n_c$, we combine the repeater protocol and the connect-and-repair protocol to get more efficient scaling. First, we use the repeater protocol to generate n_0-qubit chains with n_0 slightly larger than n_c. For instance, we can take $n_0=n_c+1$, which is a close-to-optimal choice. Then, it is straightforward to use the connect-and-repair protocol to further increase the length of the cluster starting from the n_0-qubit chains. Combining the scalings for these two protocols, we get the overall scaling rules for T and M when $n>n_c$,

$$T(n)\approx t_a(1/p)^{\log_2(n_c+1)}+(t_a/p)\log_2(n-n_c), \tag{7}$$

$$M(n)\approx(2/p)^{\log_2(n_c+1)}(n-n_c)/2. \tag{8}$$

We have shown that for any success probability p of the probabilistic entangling gate, 1D cluster states of arbitrary length can be created with efficient scaling. For universal quantum computation, however, such 1D cluster states are not sufficient. They need to be first connected and transformed into 2D cluster states (for instance, with a square lattice geometry). It is not obvious that such a connection can be done *efficiently*. First, in the connect-and-repair protocol, when an attempt fails, we need to remove the end qubits and all of their neighbors. This means that in a 2D geometry the lattice shrinks much faster to an irregular shape in the events of failure. Furthermore, a more serious obstacle is that we need to connect many more boundary qubits if we want to join two 2D cluster states. For instance, for a square lattice of n qubits, the number of boundary qubits scales as $\sqrt{n}$ (which is distinct from a 1D chain). If we need to connect all the corresponding boundary qubits of the two parts, the overall success probability is exponentially small.

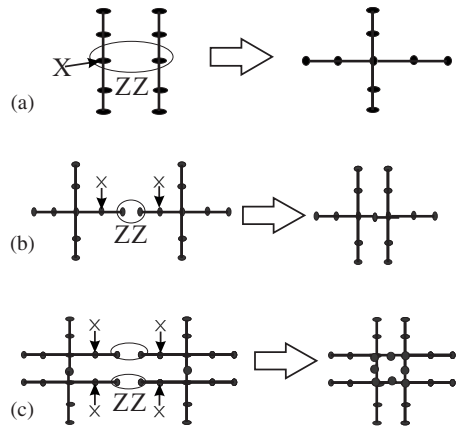

FIG. 11. Illustration of the steps for construction of the two-dimensional square lattice cluster states from a set of cluster chains. (a) Construction of the basic + shape states from cluster chains by applying a ZZ gate to connect the two middle qubits and an X measurement on one middle qubit to remove it. (b) and (c) Construction of the square lattice cluster state from the + shape states through probabilistic ZZ measurement gates along the legs and X measurements to remove the remaining redundant qubits. See Duan and Raussendorf (2005) for a similar construction with the controlled phase flip gates.

To overcome this problem, we introduce a method which enables efficient connection by attaching a long leg (a 1D cluster chain) to each boundary qubit of the 2D lattice. The protocol is divided into the following steps. First, we try to build a + shape cluster state by probabilistically connecting two cluster chains each of length $2n_l+1$ (the value of n_l is specified below). This can be done through the probabilistic ZZ gate together with a simple Hadamard gate H and an X measurement, as shown in Fig. 11(a) and explained in its caption. With on average $1/p$ repetitions, we get a + shape state with the length of each of the four legs given by n_l. We use the + shape state as the basic building blocks of large-scale 2D cluster states. In the + shape state, we have attached four long legs to the center qubit. The leg qubits serve as ancilla to generate near-deterministic connection from the probabilistic ZZ gates. The key idea here is that if we want to connect two center qubits, we always start the connection along the end qubits of one of the legs (see Fig. 11). If such an attempt fails, we can delete two end qubits and try the connection again along the same legs. If the leg is sufficiently long, we can almost certainly succeed before we reach (destroy) the center qubits. When we succeed and if there are still redundant leg qubits between the two center ones, we can delete the intermediate leg qubits by performing simple single-bit X measurements on all of them [see Figs. 10(c) and 11 for the third property of the cluster state]. With such a procedure, we can continuously connect the center qubits and form any complex lattice geometry [see the illustration for construction of the square lattice state in Figs. 11(b) and 11(c)]. What is important here is that after each time of connection of the center qubits, in the formed new shape, we still have the same length of an-

cillary legs on all the boundary qubits, which enables the succeeding near-deterministic connection of these new shapes.

Now we investigate for the 2D case how the computational overhead scales with the size of the cluster state. If the ancillary legs have length n_l, for each connection of two center qubits, we can try at most $n_l/2$ times of the probabilistic ZZ gates, and the overall success probability is given by $p_c=1-(1-p)^{n_l/2}$. If we want to build a square lattice cluster state of N qubits, we need about $2N$ times of connections of the center qubits (there are about $2N$ edges in an N-vertex square lattice). The probability for all these connections to be successful is given by p_c^{2N}. We require that this overall success probability is sufficiently large with $p_c^{2N} \geqslant 1-\epsilon$, where ϵ is a small number characterizing the overall failure probability. From that requirement, we find $n_l \simeq (2/p)\ln(2N/\epsilon)$. To construct a square lattice cluster state of N qubits, we need to consume N + shape states, and each of the latter requires on average $2/p$ cluster chains with a length of $2n_l+1$ qubits. So we need in total $2N/p$ cluster chains, each of $2n_l+1$ bits, which can be prepared in parallel with $(2N/p)M(2n_l+1)$ ZZ attempts within a time period $T(2n_l+1)$ [see Eqs. (7) and (8) for expressions of $M(n)$ and $T(n)$]. This gives the resources for preparation of all the basic building blocks (the chains). Then we need to connect these blocks to form the square lattice. We assume that the connections of all the building blocks are done in parallel. The whole connection takes on average $2N/p$ ZZ attempts and consumes a time at most t_a/p $\ln(2N/\epsilon)$. Summarizing these results, the temporal and operational resources for preparation of an N-bit square lattice cluster state are given by

$$T(N) \approx t_a(1/p)^{\log_2(4/p-2)} + \frac{t_a}{p}\ln(2N/\epsilon) + \frac{t_a}{p}\log_2\left(\frac{4}{p}[\ln(2N/\epsilon)-1]\right), \quad (9)$$

$$M(N) \approx (2/p)^{2+\log_2(4/p-2)} N[\ln(2N/\epsilon)-1] + 2N/p. \quad (10)$$

In the 2D case, the temporal and the operational overhead still shows efficient scaling with the qubit number N, logarithmically for $T(N)$ and $N\ln(N)$ for $M(N)$. Their scalings with $1/p$ are almost the same as in the 1D case except for an additional factor of $1/p^2$ for $M(N)$. Through some straightforward variations in the above method, it is also possible to efficiently prepare any complicated graph state using probabilistic ZZ gates.

Values of $T(N)/t_a$ and $M(N)$ are listed in Table I under several different success probabilities p with the qubit number $n=10^9$ and the overall failure probability $\epsilon \sim 10^{-4}$. If we take the current experimental value of $p \sim 2\times 10^{-8}$, we get ridiculously large numbers for $T(N)/t_a$ and $M(N)$. Although their scaling with N is still polynomial, the large prefactor $(1/p)^{\log_2(4/p-2)}$ makes the requirements totally impractical. With near-future improvement of the experimental technology, in particular, with a cavity in the intermediate coupling region to increase the photon collection and coupling efficiency, the success probability p could be pushed to the region of 10^{-4}–10^{-2}. With $p \sim 10^{-2}$, one can prepare cluster states of tens of qubits with $T(N)/t_a \sim 10^8$ (which is about the preparation time in current experiments), but for $n=10^9$, the required time $T(n)/t_a \sim 10^{17}$ is still too large. Desired values of p would be 5% or above. With such a success probability, one can prepare arbitrarily large cluster states with the total time bounded by $T(N)/t_a \sim 10^8$. Achieving such values of p requires significant improvement in all efficiencies for the photon collection, transmission, and detection. Different theoretical schemes for the probabilistic gates, for instance, using the type-I photon link instead of the type-II link (Duan *et al.*, 2004), can also help to increase the success probability.

TABLE I. List of the preparation time $T(N)$ (in units of pulse cycle t_a) and the total number of trials $M(N)$ at different success probabilities p for generation of a 2D cluster state with the number of qubits $N=10^9$ and the overall error probability $\epsilon=10^{-4}$.

p	2×10^{-8}	10^{-4}	10^{-2}	5%	10%
$T(N)/t_a$	10^{212}	10^{61}	10^{17}	10^{8}	1.8×10^{5}
$M(N)$	10^{247}	10^{85}	10^{35}	10^{24}	10^{20}

C. A hybrid quantum network through local deterministic gates and remote probabilistic entanglement

In Secs. III.A and III.B, we have shown that scalable quantum communication or computation networks can be realized in principle with probabilistic entangling gates. The required resources scale polynomially with the size of the network, and this cost is significant if the gate success probability is too small. In this section, we discuss an alternative approach to scalable quantum networks based on a combination of local deterministic gates and remote probabilistic entanglement, following the proposal of Duan *et al.* (2004). This hybrid approach requires the ability to perform local deterministic gates on adjacent ions, whose fidelity must exceed appropriate error-correction thresholds. For the trapped ion system, given recent experimental advances (Benhelm *et al.*, 2008; Blatt and Wineland, 2008), it appears possible to meet such thresholds using local Coulomb gates. With this additional capability, the scaling for large-scale quantum networks becomes more efficient and realistic for even very small probabilistic gate success rates.

The simplest version of a hybrid trapped ion network consists of quantum registers, each with a pair of ions that can be manipulated separately with laser beams. To achieve sufficient individual addressing, the two ions in each register could be spatially resolved with tightly focused laser beams (Nägerl *et al.*, 1999), spectrally resolved using different ion isotopes or species (Blinov *et al.*, 2002; Barrett *et al.*, 2003), or the ions could be spatially separated in different trap regions where they can

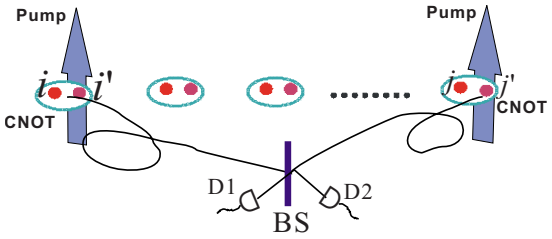

FIG. 12. (Color online) Schematic of a quantum computational model based on a hybrid approach. The ancilla ions in different traps are entangled through the probabilistic entangling protocol. Deterministic gates on remote ions are constructed from the local Coulomb gates and the probabilistic remote entanglement.

be brought together for local Coulomb gates (Kielpinski *et al.*, 2002). Within each pair, one ion (the logic ion) encodes the quantum information and the second ion (the ancilla) allows the coupling to another ion pair through a probabilistic photonic entangling protocol. This probabilistic entanglement, combined with the local Coulomb gates within each pair, allows for an effective quantum gate between the remote logical qubits.

The resulting remote operation is deterministic because the probabilistic entangling operations can be done offline, and the failure of any individual entangling attempt does not destroy the computational quantum state carried by the logical ions. When the probabilistic entanglement protocols are attempted simultaneously between all registers, the offline waiting time scales only logarithmically with the number of registers: $T_{\text{wait}} \sim T_0 \ln(N)$.

1. Hybrid quantum computational network

First, we show how to use this hybrid approach to construct a scalable quantum computational network. Figure 12 shows the schematic setup. Different ion pairs can be in different traps that are separated with an arbitrary distance. Each qubit is represented by a pair of ions, denoted as i and i' for the logic ion and the ancilla ion, respectively. We need to perform deterministic quantum gates between two arbitrary logic ions in different traps. For this purpose, we assume that each ancilla ion is connected to a single-photon detector, possibly through an optical fiber. To entangle two ancilla ions, say, i' and j', we pump both to excited electronic states with appropriate resonant laser beams. The resulting spontaneously emitted photons from these two ions are directed to single-photon detectors for a Bell-type collective measurement. For particular measurement results, the two ancilla ions i' and j' will be projected into a Bell state, which we denote as $|\Phi\rangle_{i'j'}=(|01\rangle+|10\rangle)/\sqrt{2}$ (see Sec. III.C for the entangling protocol). Each entangling operation succeeds with a probability p_s (the probability to register the appropriate result), so we need to repeat this operation on average $1/p_s$ times for a final successful confirmation of entanglement, with the total preparation time about t_a/p_s, where again t_a is the time for each individual entangling attempt. The logic and ancilla ions are individually resolved so that the probabilistic entangling operation on the ancilla ions does not influence the logic ions even if this entangling operation fails.

With assistance of the Bell state $|\Phi\rangle_{i'j'}$, we can achieve remote quantum controlled-NOT (CNOT) gates on the logic ions i and j. We assume that quantum CNOT gates can be realized on the local ions i,i' and j,j' in the same pairs through the conventional Coulomb gate (Cirac and Zoller, 1995; Monroe, 2002; Blatt and Wineland, 2008). These local CNOT gates are denoted by $C_{ii'}$ and $C_{jj'}$, where the subscripts refer to the control and target ions. We can achieve the remote CNOT gate C_{ij} on the logic ions i,j through a combination of the gates $C_{ii'}$, $C_{jj'}$ and the Bell state $|\Phi\rangle_{i'j'}$. This can be seen by considering the following identity:

$$\begin{aligned} C_{ii'}C_{jj'}(|\Psi\rangle_{ij\cdots}\otimes|\Phi\rangle_{i'j'}) &= |0+\rangle_{i'j'}\otimes C_{ij}(|\Psi\rangle_{ij\cdots}) + |0-\rangle_{i'j'}\otimes Z_iC_{ij}(|\Psi\rangle_{ij\cdots}) \\ &\quad + |1+\rangle_{i'j'}\otimes X_jC_{ij}(|\Psi\rangle_{ij\cdots}) + |1-\rangle_{i'j'} \\ &\quad \otimes(-Z_iX_j)C_{ij}(|\Psi\rangle_{ij\cdots}), \end{aligned} \tag{11}$$

where $|\pm\rangle_{j'}=(|0\rangle_{j'}\pm|1\rangle_{j'})/\sqrt{2}$ and $|\Psi\rangle_{ij\cdots}$ denotes the computational state for which the i,j ions may be entangled with other logic ions. The single-qubit Pauli operators Z_i and X_j act on the corresponding ions i,j. The above identity has been used in different contexts, in particular, for discussion of the communication complexity of the quantum CNOT gate (Sorensen and Molmer, 1998; Gottesman, 1999). This identity shows that to perform a remote CNOT gate C_{ij} on the logic ions i,j, we can take the following steps:

- Prepare the ancilla ion i' and j' into the electron paramagnetic resonance state $|\Phi\rangle_{i'j'}$ using a probabilistic entangling protocol. Repeat the protocol until it succeeds.
- Apply the local motional CNOT gates $C_{ii'}$ and $C_{jj'}$ on the ions i,i' and j,j' within the same pairs.
- Measure the ancilla ion i' in the basis $\{|0\rangle_{i'},|1\rangle_{i'}\}$ and the ancilla ion j' in the basis $\{|+\rangle_{j'},|-\rangle_{j'}\}$.
- Apply a single-bit rotation $\{I,Z_i,X_j,-Z_iX_j\}$ on ion i and/or j if we get the measurement results $\{0+,0-,1+,1-\}$, respectively.

The resulting remote quantum CNOT gate C_{ij} is deterministic despite that the seeding entanglement operations may have been established probabilistically. When accompanied by simple local single-bit rotations, this hybrid computation model is therefore scalable, with no fundamental limit to the number of ion-pair nodes. The essential resources for this approach are two-qubit local Coulomb gates and remote ion-ion probabilistic entanglement, both of which have been achieved in the laboratory.

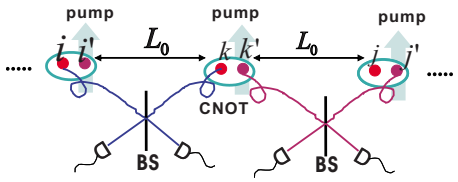

FIG. 13. (Color online) Schematic realization of quantum repeaters with trapped ions based on a combination of the probabilistic detection-induced remote entanglement and the local Coulomb gates.

2. Hybrid quantum repeater network

With the same system, we can also realize a quantum repeater network. Figure 13 shows schematically the implementation of quantum repeaters with the paired-ion setup. With the probabilistic entangling protocol, we can generate entanglement between two nodes, say, i and k, and also k' and j', each with a communication distance L_0 which is comparable to the photon attenuation length. The success probability for the preparation of each segment of entanglement is given by $p=p_s p_a$, where p_s is the inherent success probability of the entangling protocol and $p_a=e^{-\alpha L_0}$ is the photon attenuation in the channel. These two segments of entanglement can be connected to generate an entangled state between i and j' through a local collective Bell measurement on the two ions k and k' in the same pair. A combination of the Coulomb CNOT gate and individual ion detections achieves the desired collective measurement.

The preparation time for each segment of entanglement is $T_g \approx t_a/p$, and the time for establishing entanglement between the next neighboring nodes i and j (with a distance $2L_0$) is given by $T_2 \approx 2T_g$ ($T_2 \approx T_g$) if we prepare each segment of entanglement sequentially (in parallel). So the time required for establishing entanglement over n segments with a total communication distance of nL_0 is given by $T_n \approx nT_g \approx ne^{\alpha L_0}(t_a/p_s)$ (or $T_n \approx T_g$ for the parallel preparation) with this hybrid approach.

In the above, we have assumed the simplest form of quantum register, each consisting of only two ions. If we allow a few more ions in each quantum register, the above approach can be extended considerably by incorporating protocols to purify the entanglement established over remote trapped ion qubits (Liang *et al.*, 2007).

IV. OUTLOOK

Individual trapped ions are known as the most advanced material qubit, as they can be localized in one place for extended periods like a solid while interacting weakly with their environment. But trapped ions are also attractive candidates for quantum networking applications because they can be replicated in different nodes with nearly identical characteristics, which can be an important practical feature for the implementation of photonic quantum networks. While the coupling of trapped ion qubits to photons is typically small, this is not a fundamental shortcoming as there exist probabilistic protocols for the scalable photonic networking of trapped ion qubits. It is possible to generate scalable entangled states of many ions through the use of exclusively probabilistic gates, although this will likely require gate success probabilities to approach $p \sim 10^{-3}$ or higher. On the other hand, when probabilistic gates are combined with local deterministic gates, a natural situation for small ion crystals that can be entangled based on their Coulomb interaction, scalable quantum information processing can proceed with gate success probabilities that are even smaller.

Recent experiments have shown the basic features of photonic networking between separated single trapped ions, and future technological gains in ion trap photonics may dramatically increase the probabilistic gate success rate. Future ion-photonic interfaces will likely exploit advances in microfabricated ion trap structure (Blatt and Wineland, 2008) and integrated optical elements. One example of an ion-photonic network architecture is

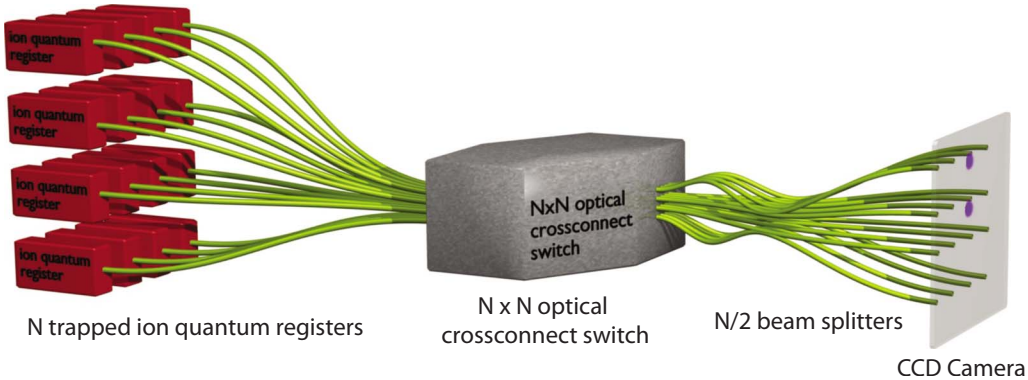

FIG. 14. (Color online) Hierarchical trapped ion quantum computer. N quantum registers (left) each consists of a many-qubit crystal of trapped ions that can be entangled through deterministic Coulomb gates. One ion within each register is coupled optically to an $N \times N$ optical cross-connect switch in order to propagate quantum information between registers and create large-scale entangled states among all ions. Such a hierarchical approach to scaling the ion-photon network may allow the scaling to millions or more trapped ion qubits.

shown in Fig. 14, where registers of trapped ion crystals allow local entanglement to proceed though conventional Coulomb gates, and entanglement between registers is accomplished through the interference of synchronously emitted photons from selected ions through the use of a reconfigurable $N \times N$ optical cross-connect switch. Such a hierarchical architecture is promising for the scaling to very large numbers of trapped ion qubits. There are many other possible architectures, taking the lead from interconnects in classical processors.

We note finally that while trapped ions are among the best controlled matter qubits today, in the future it should be possible to apply the optical protocols discussed in this Colloquium to other optically active qubits. For instance, the same protocols apply to neutral atoms in an optical trap (Volz *et al.*, 2006). Furthermore, recent experimental progress has shown the manipulation of local electron-spin and nuclear-spin qubits in nitrogen-vacancy color-center impurities in diamond (Dutt *et al.*, 2007; Neumann *et al.*, 2008). All of the protocols discussed in this Colloquium could ultimately be applied to the *NV*-diamond system, as well as other optically active solid-state qubits such as a large class of rare-earth ion-doped solid-state systems. Such quantum registers can also be represented by single semiconductor quantum dots, where the two local qubits are carried by the electron- and nuclear-spin states. The electron-spin states can be coupled to photons, and separated dots can be entangled through the probabilistic entangling protocols discussed above. The local gates on the electron spin and the nuclear spin could be achieved with laser manipulation of the hyperfine interaction.

ACKNOWLEDGMENTS

It is a great pleasure to acknowledge our collaborators for the works described in this Colloquium. We thank, in particular, Sean Barrett, Boris Blinov, Ignacio Cirac, David Hayes, Jungsang Kim, Jeff Kimble, Rudy Kohn, Peter Kok, Alex Kuzmich, Mikhail Lukin, Le Luo, Martin Madsen, Dzmitry Matsukevich, Peter Maunz, David Moehring, Steven Olmschenk, Robert Raussendorf, Christoph Simon, John Sterk, Jake Taylor, Kelly Younge, and Peter Zoller for fruitful collaboration, enlightening discussions, and insightful comments. This work was supported by the USAFOSR through a MURI program, the DARPA OLE program, the IARPA/USARO quantum computation program, the NSF PIF program, and the Physics Frontier Center at JQI.

REFERENCES

Balzer, C., A. Braun, T. Hannemann, C. Paape, M. Ettler, W. Neuhauser, and C. Wunderlich, 2006, Phys. Rev. A **73**, 041407(R).

Barrett, M. D., B. DeMarco, T. Schaetz, V. Meyer, D. Leibfried, J. Britton, J. Chiaverini, W. M. Itano, B. Jelenkovi, J. D. Jost, C. Langer, T. Rosenband, and D. J. Wineland, 2003, Phys. Rev. A **68**, 042302.

Barrett, S. D., and P. Kok, 2005, Phys. Rev. A **71**, 060310(R).

Benhelm, J., G. Kirchmair, C. F. Roos, and R. Blatt, 2008, Nat. Phys. **4**, 463.

Bennett, C. H., *et al.*, 1993, Phys. Rev. Lett. **70**, 1895.

Bennett, C. H., *et al.*, 1996, Phys. Rev. Lett. **76**, 722.

Beugnon, J., M. P. A. Jones, J. Dingjan, B. Darquie, G. Messin, A. Browaeys, and P. Grangier, 2006, Nature (London) **440**, 779.

Blatt, R., and D. Wineland, 2008, Nature (London) **453**, 1008.

Blatt, R., and P. Zoller, 1988, Eur. J. Phys. **9**, 250.

Blinov, B. B., D. L. Moehring, L.-M. Duan, and C. Monroe, 2004, Nature (London) **428**, 153.

Blinov, B. B., *et al.*, 2002, Phys. Rev. A **65**, 040304.

Bollinger, J. J., D. J. Heinzen, W. M. Itano, S. L. Gilbert, and D. J. Wineland, 1991, IEEE Trans. Instrum. Meas. **40**, 126.

Braunstein, S. L., and A. Mann, 1995, Phys. Rev. A **51**, R1727.

Briegel, H.-J., W. Duer, J. I. Cirac, and P. Zoller, 1998, Phys. Rev. Lett. **81**, 5932.

Briegel, H.-J., and R. Raussendorf, 2001, Phys. Rev. Lett. **86**, 910.

Cabrillo, C., J. I. Cirac, P. García-Fernández, and P. Zoller, 1999, Phys. Rev. A **59**, 1025.

Chaneliere, T., D. N. Matsukevich, S. D. Jenkins, S.-Y. Lan, R. Zhao, T. A. B. Kennedy, and A. Kuzmich, 2007, Phys. Rev. Lett. **98**, 113602.

Cirac, J. I., and P. Zoller, 1995, Phys. Rev. Lett. **74**, 4091.

Cirac, J. I., P. Zoller, H. J. Kimble, and H. Mabuchi, 1997, Phys. Rev. Lett. **78**, 3221.

DeVoe, R. G., and R. G. Brewer, 1996, Phys. Rev. Lett. **76**, 2049.

Duan, L.-M., B. B. Blinov, D. L. Moehring, and C. Monroe, 2004, Quantum Inf. Comput. **4**, 165.

Duan, L. M., J. I. Cirac, and P. Zoller, 2002, Phys. Rev. A **66**, 023818.

Duan, L.-M., M. D. Lukin, J. I. Cirac, and P. Zoller, 2001, Nature (London) **414**, 413.

Duan, L.-M., M. J. Madsen, D. L. Moehring, P. Maunz, R. N. Kohn, and C. Monroe, 2006, Phys. Rev. A **73**, 062324.

Duan, L.-M., and C. Monroe, 2007, Adv. At., Mol., Opt. Phys. **55**, 419.

Duan, L.-M., and R. Raussendorf, 2005, Phys. Rev. Lett. **95**, 080503.

Duan, L.-M., B. Wang, and H.-J. Kimble, 2005, Phys. Rev. A **72**, 032333.

Dutt, M. V., L. Gurudev, L. Childress, E. Jiang, J. Togan, J. Maze, F. Jelezko, A. S. Zibrov, P. R. Hemmer, and M. D. Lukin, 2007, Science **316**, 1312.

Eichmann, U., J. C. Bergquist, J. J. Bollinger, J. M. Gilligan, W. M. Itano, D. J. Wineland, and M. G. Raizen, 1993, Phys. Rev. Lett. **70**, 2359.

Felinto, D., C. W. Chou, J. Laurat, E. W. Schomburg, H. de Riedmatten, and H. J. Kimble, 2006 Nat. Phys. **2**, 841.

Gerber, S., D. Rotter, M. Hennrich, R. Blatt, F. Rohde, C. Schuck, M. Almendros, R. Gehr, F. Dubin, and J. Eschner, 2009, New J. Phys. **11**, 013032.

Gisin, N., G. Ribordy, W. Tittel, and H. Zbinden, 2002, Rev. Mod. Phys. **74**, 145.

Gottesman, D., 1999, in *Proceedings of the XXII International Colloquium on Group Theoretical Methods in Physics*, edited by S. P. Corney, R. Delbourgo, and P. D. Jarvis (International, Cambridge, MA), pp. 32–43.

Hein, M., W. Dür, J. Eisert, R. Raussendorf, M. Van den Nest, and H.-J. Briegel, 2006, *Quantum Computers, Algorithms and Chaos*, edited by G. Casati, D. L. Shepelyansky, P. Zoller,

and G. Benenti, Proceedings of the International School of Physics "Enrico Fermi," Varenna, 2005 (IOS, Varenna).
Hong, C. K., Z. Y. Ou, and L. Mandel, 1987, Phys. Rev. Lett. **59**, 2044.
James, D. F. V., P. G. Kwiat, W. J. Munro, and A. G. White, 2001, Phys. Rev. A **64**, 052312.
Kaltenbaek, R., B. Blauensteiner, M. Zukowski, M. Aspelmeyer, and A. Zeilinger, 2006, Phys. Rev. Lett. **96**, 240502.
Kielpinski, D., C. Monroe, and D. Wineland, 2002, Nature (London) **417**, 709.
Kimble, H.-J., 2008, Nature (London) **453**, 1023.
Kuzmich, A., W. P. Bowen, A. D. Boozer, A. Boca, C. W. Chou, L.-M. Duan, and H. J. Kimble, 2003, Nature (London) **423**, 731.
Legero, T., T. Wilk, M. Hennrich, G. Rempe, and A. Kuhn, 2004, Phys. Rev. Lett. **93**, 070503.
Liang, L., J. M. Taylor, A. S. Sorensen, and M. D. Lukin, 2007, Phys. Rev. A **76**, 062323.
Lim, Y. L., S. D. Barrett, A. Beige, P. Kok, and L. C. Kwek, 2006, Phys. Rev. A **73**, 012304.
Luo, L., D. Hayes, T. A. Manning, D. N. Matsukevich, P. Maunz, S. Olmschenk, J. D. Sterk, and C. Monroe, 2009, e-print arXiv:0906.1032, Fortschr. Phys. (to be published).
Madsen, M. J., D. L. Moehring, P. Maunz, Jr., R. N. Kohn, L.-M. Duan, and C. Monroe, 2006, Phys. Rev. Lett. **97**, 040505.
Matsukevich, D. N., P. Maunz, D. L. Moehring, S. Olmschenk, and C. Monroe, 2008, Phys. Rev. Lett. **100**, 150404.
Maunz, P., D. L. Moehring, S. Olmschenk, K. C. Younge, D. N. Matsukevich, and C. Monroe, 2007, Nat. Phys. **3**, 538.
Maunz, P., S. Olmschenk, D. Hayes, D. N. Matsukevich, L.-M. Duan, and C. Monroe, 2009, e-print arXiv:0902.2136.
Michler, M., K. Mattle, H. Weinfurter, and A. Zeilinger, 1996, Phys. Rev. A **53**, R1209.
Miller, A. J., S.-W. Nam, J. M. Martinis, and A. V. Sergienko, 2003, Appl. Phys. Lett. **83**, 791.
Moehring, D. L., M. J. Madsen, B. B. Blinov, and C. Monroe, 2004, Phys. Rev. Lett. **93**, 090410.
Moehring, D. L., M. J. Madsen, K. C. Younge, R. N. Kohn, Jr., P. Maunz, L.-M. Duan, C. Monroe, and B. Blinov, 2007, J. Opt. Soc. Am. B **24**, 300.
Moehring, D. L., P. Maunz, S. Olmschenk, K. C. Younge, D. N. Matsukevich, L.-M. Duan, and C. Monroe, 2007, Nature (London) **449**, 68.
Monroe, C., 2002, Nature (London) **416**, 238.
Nägerl, H. C., D. Leibfried, H. Rohde, G. Thalhammer, J. Eschner, F. Schmidt-Kaler, and R. Blatt, 1999, Phys. Rev. A **60**, 145.
Neumann, P., N. Mizuochi, F. Rempp, P. Hemmer, H. Watanabe, S. Yamasaki, V. Jacques, T. Gaebel, F. Jelezko, and J. Wrachtrup, 2008, Science **320**, 1326.
Nielsen, M. A., and I. L. Chuang, 2000, *Quantum Computation and Quantum Information* (Cambridge University Press, Cambridge).
Olmschenk, S., D. N. Matsukevich, P. Maunz, D. Hayes, L.-M. Duan, and C. Monroe, 2009, Science **323**, 486.
Olmschenk, S., K. C. Younge, D. L. Moehring, D. N. Matsukevich, P. Maunz, and C. Monroe, 2007, Phys. Rev. A **76**, 052314.
Raussendorf, R., and H. J. Briegel, 2001, Phys. Rev. Lett. **86**, 5188.
Sackett, C. A., D. Kielpinski, B. E. King, C. Langer, V. Meyer, C. J. Myatt, M. Rowe, Q. A. Turchette, W. M. Itano, D. J. Wineland, and C. Monroe, 2000, Nature (London) **404**, 256.
Santori, C., D. Fattal, J. Vuckovic, G. S. Solomon, and Y. Yamamoto, 2002, Nature (London) **419**, 594.
Schnorrberger, U., J. D. Thompson, S. Trotzky, R. Pugatch, N. Davidson, S. Kuhr, and I. Bloch, 2009, Phys. Rev. Lett. **103**, 033003.
Shih, Y. H., and C. O. Alley, 1988, Phys. Rev. Lett. **61**, 2921.
Sorensen, A. S., and K. Molmer, 1998, Phys. Rev. A **58**, 2745.
Staudt, M. U., M. Afzelius, H. de Riedmatten, S. R. Hastings-Simon, C. Simon, R. Ricken, H. Suche, W. Sohler, and N. Gisin, 2007, Phys. Rev. Lett. **99**, 173602.
Thompson, J. K., J. Simon, H. Loh, and V. Vuletic, 2006, Science **313**, 74.
Volz, J., M. Weber, D. Schlenk, W. Rosenfeld, J. Vrana, K. Saucke, C. Kurtsiefer, and H. Weinfurter, 2006, Phys. Rev. Lett. **96**, 030404.
Wootters, W. K., 1998, Phys. Rev. Lett. **80**, 2245.
Wootters, W. K., and W. H. Zurek, 1982, Nature (London) **299**, 802.
Yurke, B., S. L. McCall, and J. R. Klauder, 1986, Phys. Rev. A **33**, 4033.